Optics Communications 430 (2019) 14–23

Contents lists available at ScienceDirect

Optics Communications

journal homepage: www.elsevier.com/locate/optcom

A novel approach based on simulation of tunable MEMS diaphragm for extrinsic Fabry–Perot sensors

Sekip Esat Hayber [a], Timucin Emre Tabaru [b], Omer Galip Saracoglu [b,c,*]

[a] Department of Electronic and Automation, Ahi Evran University, Kirsehir 40300, Turkey
[b] Clinical Engineering Research and Application Center, Erciyes University, Kayseri 38039, Turkey
[c] Department of Electrical and Electronic Engineering, Erciyes University, Kayseri 38039, Turkey

ARTICLE INFO

Keywords:
Diaphragm-based fiber optic sensors
Extrinsic Fabry–Perot interferometry (EFPI)
Finite element method (FEM)
Microelectromechanical systems (MEMS)
Acoustic pressure

ABSTRACT

A new tunable structure with a Three Leaf Clover (TLC) geometry has been proposed for use in diaphragm-based acoustic pressure sensors. The sensitivity and frequency response of this new structure, which will be an alternative to conventional circular diaphragms, was accomplished using Finite Element Method (FEM) and numerical analysis techniques. As a result of the analysis, sensitivity and frequency response approaches were obtained for the tunable-TLC structure. These approaches provide researchers to design diaphragms more convenient. Conventional circular diaphragms can be easily converted to TLC diaphragms by means of micro-electromechanical systems (MEMS) thus can be tuned up to 5 times for sensitivity and up to 1/3 times the fundamental frequency without altering the thickness and radius of the diaphragm. Obtained approach expressions were compared with FEM results for practical design purposes in a wide range of tunable parameters, and the average errors were below 2.5% for the sensitivity and below 0.5% for the fundamental frequency response, respectively.

1. Introduction

Diaphragm-based fiber optic sensors have been utilized in many application areas due to their high sensitivity, small size, immunity to electromagnetic interference, flexibility, easy adaptability to construction, low energy consumption and resistance to severe environmental conditions. Some of these are biomedical [1,2], gas detection [3–5], underwater applications [6–8], infrasound [3,9,10] and ultrasound applications [8,11,12], acoustics [13–16], pressure [17–19], acoustic pressure [20–22], and partial discharge [23–25].

Diaphragm-based sensors are most commonly consisted of with the principle of Extrinsic Fabry–Perot Interferometry (EFPI) [2]. Similarly, the most common use of the Fabry–Perot (FP) interferometry is in diaphragm-based applications where one of the two reflective surfaces is formed with a diaphragm [19–26]. Since the diaphragm is the most important part of the diaphragm-based EFPI fiber acoustic pressure sensors [27], the operating performance of the sensor is directly determined by the diaphragm design. The most important parameters affecting this performance are operating range, sensitivity, linearity and tunability. These are achieved by center deflection and frequency response analysis, which are the two most important characters of the diaphragm [12]. Sensitivity and frequency response of the sensor can be adjusted by changing the thickness and surface length of the diaphragm. For example, reducing the thickness of the diaphragm increases sensitivity, however, this situation may not suitable for each diaphragm material, because it is a difficult process to produce the diaphragm in sub-micrometer thickness for the most commonly used silicon or silica materials [18,21]. Although another way to increase sensitivity is to increase the surface length of the diaphragm, this results in large sensing tips which are not useful for sensor miniaturizations. In many studies, the effect of diameter on the frequency and sensitivity has not been utilized since the inner diameter (125 μm) of the standard ceramic ferrules determines the size of the diaphragm [11,18,21,25]. Considering these restrictions, one can conclude that tuning can be made much easier with geometries that have parameters other than thickness and surface length. With the aid of the developing Micro Electromechanical Systems (MEMS), it is easy to produce diaphragms in desired geometries [23,24,28,29].

In this study, the sensitivity and frequency response of the diaphragm geometry proposed as Three Leaf Clover (TLC) with an innovative approach to conventional circular diaphragm geometry is analyzed by Finite Element Method (FEM) and analytical methods. As a result of FEM and theoretical analysis, an approximate expression is developed

* Corresponding author at: Department of Electrical and Electronic Engineering, Erciyes University, Kayseri 38039, Turkey.
E-mail addresses: sehayber@ahievran.edu.tr (S.E. Hayber), etabaru@erciyes.edu.tr (T.E. Tabaru), saracog@erciyes.edu.tr (O.G. Saracoglu).

https://doi.org/10.1016/j.optcom.2018.08.021
Received 23 May 2018; Received in revised form 8 August 2018; Accepted 9 August 2018
Available online 13 August 2018
0030-4018/

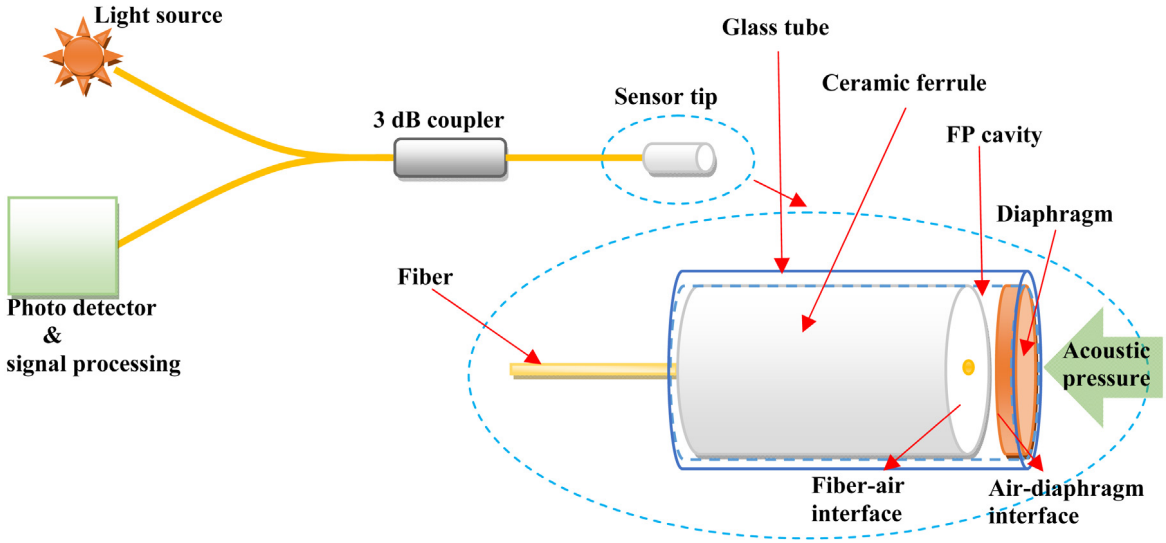

Fig. 1. The structure of diaphragm-based fiber optic EFPI sensor system.

for the TLC-shaped diaphragm. Thus, it is aimed to provide ease of design for sensor sensitivity and operating frequency. It has also become possible to produce tips with different frequency and sensitivity values without changing the diaphragm diameter and thickness. It has been shown that the sensitivity and the fundamental resonance frequency of the current sensor can be adjusted to 5 times and 1/3 times the desired value, respectively, without changing the diameter and thickness values, thanks to the proposed geometry.

2. Materials and methods

2.1. Conventional diaphragm geometry

Optical interference theory and diaphragm dynamic vibration analysis constitute the two basic principles of diaphragm-based EFPI sensors. The optic intensity at the sensor output is determined by the two basic mechanisms, which are optical interference theory and diaphragm dynamic vibration analysis. Fig. 1 shows that operating principle of this sensor system, which consists of a sensor tip, a semiconductor light emitter capable of operating in different wave lengths, an optical receiver and fibers providing the connection between the components. A 3 dB fiber coupler is used to receive the reflected signal and reduce the optical feedback which comes back to the source. The sensor tip consists of two interfaces, the first one is the fiber–air interface and the other one is the air–diaphragm interface. When the light beam emerging from the light source reaches the sensor tip, it encounters two the different interfaces. A part of the light is reflected from the first interface and the remaining part reaches the diaphragm surface through the air gap. A large part of the light beam is also reflected from the second interface and comes back to the first interface and enters the fiber. The light beam entering the fiber reaches the photodetector via passing through the circulator [25]. The detector converts the light beam to the electrical signal and transfers it to the signal processing unit. Thus, when the diaphragm is exposed to an acoustic pressure while continuous multiple reflections continue, a change in FP cavity occurs because of flexing of the diaphragm. The change in the FP cavity causes a variation in the phase of the light and this variation in phase affects the optic intensity at the output through the interferometer. Detection is achieved when the optic intensity at the output is related to the acoustic pressure acting on the diaphragm surface.

Diaphragm-based EFPI sensors are based on the dynamic vibration analysis of diaphragms in addition to the above-mentioned optical interference theory [19,23,25]. The mechanical properties and geometric dimensions of the diaphragm material determine the sensitivity and frequency response of the sensor system to acoustic pressure. The sensitivity and frequency response of the sensor must match the measurand. This is achieved if a diaphragm is designed which is sensitive to the intensity and frequency of the acoustic pressure. Under applied pressure, the center deflection of a circular and rigidly clamped round diaphragm is given by [29]:

$$d = \frac{3\left(1-\upsilon^2\right)Pr^4}{16Et^3} \tag{1}$$

where υ is Poisson's ratio, P is applied pressure, E is Young's modulus, r and t are radius and thickness of the diaphragm, respectively. The amount of the deflection at the center of the diaphragm depends on the mechanical properties (i.e., υ and E) of the diaphragm material and geometric dimensions (i.e., r and t). The sensitivity (S) to the amount of the deflection under unit pressure is defined by [10]:

$$S = \frac{d}{P} \tag{2}$$

The sensitivity increases with increasing amount of the radius and decreases with increasing thickness. The fundamental natural frequency of a circular and fixed diaphragm is [14]:

$$f = \frac{10.21t}{2\pi r^2}\sqrt{\frac{E}{12\rho(1-\upsilon^2)}} \tag{3}$$

where ρ is the mass density of the diaphragm. Sensitivity, as well as the frequency response, depends on the material properties and geometric dimensions. The effect of the radius and the thickness on the frequency is the opposite of the effect on sensitivity. That is, while the increasing amount of radius reduces the frequency, the increased amount of thickness increases the frequency.

2.2. New geometric approach for diaphragm design

The design of the sensors at the desired frequency and sensitivity values is of great importance for the detection of the measurand. For example, to obtain narrowband and high sensitivity acoustic sensors, the sensor should be operated the values where close to the resonance frequency. In some cases, diaphragm-based EFPI sensors require a wide range of flat frequency response, which must be at least three to five times greater than the highest frequency value of measured frequency [29]. Similarly, sensors that will detect infrasound [10] and ultrasound [8] signals should have different sensitivities. To achieve this, there are different diaphragm geometries in the literature [12,23,24,30,31], although, these geometries are not as common

Fig. 2. The structure of diaphragms (a) TLC (b) Conventional circular.

Table 1
Sensitivity S (nm/kPa) of TLC for $r_i = r_o/2$ and Circular Diaphragms (CD).

r_o(μm)	Thickness t = 5 μm		Thickness t = 10 μm		Thickness t = 15 μm		Thickness t = 20 μm	
	CD	TLC α = 120° to 10°	CD	TLC α = 120° to 10°	CD	TLC α = 120° to 10°	CD	TLC α = 120° to 10°
300	160.93	160.93–564.40	19.98	19.98–71.17	5.97	5.97–21.23	2.53	2.53–9.05
400	509.92	509.92–1762.8	63.69	63.69–221.75	18.78	18.78–66.09	7.88	7.88–27.98
500	1244.3	1244.3–4249.1	155.50	155.50–535.03	45.85	45.85–158.97	19.31	19.31–67.53
600	2582.8	2582.8–8714.0	321.86	321.86–1096.2	94.85	94.85–326.44	40.26	40.26–138.27
700	4779.7	4779.7–15913	597.98	597.98–2011.5	176.95	176.95–597.52	74.38	74.38–253.36

as circular diaphragms. Circular geometries are very common due to the fact that they are compatible with standard fiber components and the mathematical models are available [3,4,6,10,27,11,13–16,18–22]. Many researchers used Eqs. (1) and (3) when performing diaphragm designs [10,14,25,29]. The sensitivity and the frequency response of the conventional circular diaphragm are controlled by two geometric dimensions (Fig. 2b). Since, the limitations mentioned in Section 1 can occur for both parameters, there is need for tunable structures with different sensitivity range and frequency responses by including the influence of other design parameters.

In our study, a diaphragm geometry in the form of a Three Leaf Clover (TLC) is shown in Fig. 2a. This structure will have higher tunability because it contains more parameters than the conventional circular geometry. Due to the introduced geometry, sensor tips with different sensitivity and frequency ranges can be produced in cases where the diaphragm thickness and diameter cannot be changed. Contrary to other studies, the proposed TLC geometric approach confirms itself by reaching the conventional diaphragm structure at the limit values. Another interesting advantage of the new geometry is that there will be no need for additional external air hole to compensate the external and internal pressures [3,4,13,22].

3. Numerical analysis

Different numerical values were selected describing the TLC diaphragm, outer radius r_o, inner radius r_i, thickness t and leaf angle α. Finite Element Method (FEM) based numerical simulation was performed by using static structural analysis to examine the effects of these parameters on the deformation reaction and modal analysis was performed for the frequency response. The effects of TLC diaphragm parameters on sensor sensitivity and frequency response were investigated. Finally, diaphragm deflection and frequency response equations were produced as a result of these analyzes.

In the analyzes, silica (SiO_2) was selected as the diaphragm material. Since our main goal in this work is to develop a general approximation model, the parameters have been chosen over a wide range. In other words, the diaphragms to be produced with the selected parameters will have very different sensitivity ratings.

3.1. Static structural analysis of diaphragm deflection

For the diaphragms formed with thicknesses t of 5, 10, 15 and 20 μm, and the outer radius r_o values are chosen as 300, 400, 500, 600 and 700 μm, respectively. During the analysis, the inner radius r_i is increased up to the outer radius, and the leaf angle α values were increased from 10° to 110° with 10° of steps. The obtained static structural analysis results are shown in Figs. 3 and 4 for the thickness values of 10 μm and 15 μm, respectively.

As seen in Figs. 3 and 4, the sensitivity decreases with increasing the diaphragm thickness and decreasing the diaphragm outer radius. It is determined that there is a proportion of $S \propto 1/t^3$ between sensitivity and thickness. In addition, there is also a proportion of $S \propto r_o^4$ between sensitivity and outer radius. This is also compatible with Eq. (1), which is applied to conventional circular diaphragms (CD). Thus, the effect of the thickness and the radius on the circular geometries are valid for the TLC diaphragm. When the inner radius is chosen to be equal to half of the outer radius or greater than half of the outer radius, $r_i \geq r_o/2$, the results come close to each other. From the numerical results obtained, it is determined that there is a proportion of $S \propto 1/\sqrt{\alpha}$ is between the leaf angle and sensitivity. Also, when inner radius is equal to half of outer radius, $r_i = r_o/2$, the dynamic range reaches the highest value. The general nature of the graphs created for diaphragms with thickness of 5 μm and 20 μm is similar to those given in Figs. 3 and 4. Thus these interpretations are also valid for diaphragms with thickness of 5 μm and 20 μm. By changing these parameters, diaphragms with a degree of sensitivity that scan a very large scale have been created. This situation is shown in Table 1. For example, the first row of Table 1 summarizes that the sensitivity for t = 5 μm and r_o = 300 μm can be tuned between 160.93–564.40 nm/kPa for TLC diaphragm while it remains constant at 160.93 nm/kPa for CD diaphragm.

3.2. Modal analysis of diaphragm natural frequency

For the diaphragms formed with thicknesses t of 5, 10, 15 and 20 μm, and the outer radius r_o values are chosen as 300, 400, 500, 600 and 700 μm, respectively. During the modal analysis, the inner radius r_i is increased up to the outer radius, and the leaf angle α values are increased from 10° to 110° with 10° of steps. The obtained modal analysis results are shown in Figs. 5 and 6 for the thickness values of 10 μm and 15 μm, respectively. The general nature of the graphs created for diaphragms with thickness of 5 μm and 20 μm is similar to those given in Figs. 5 and 6.

As can be seen from Figs. 5 and 6, the fundamental resonance frequency increases with increasing thickness of the diaphragm, and there is a proportion of $f \propto t$ between the fundamental resonance

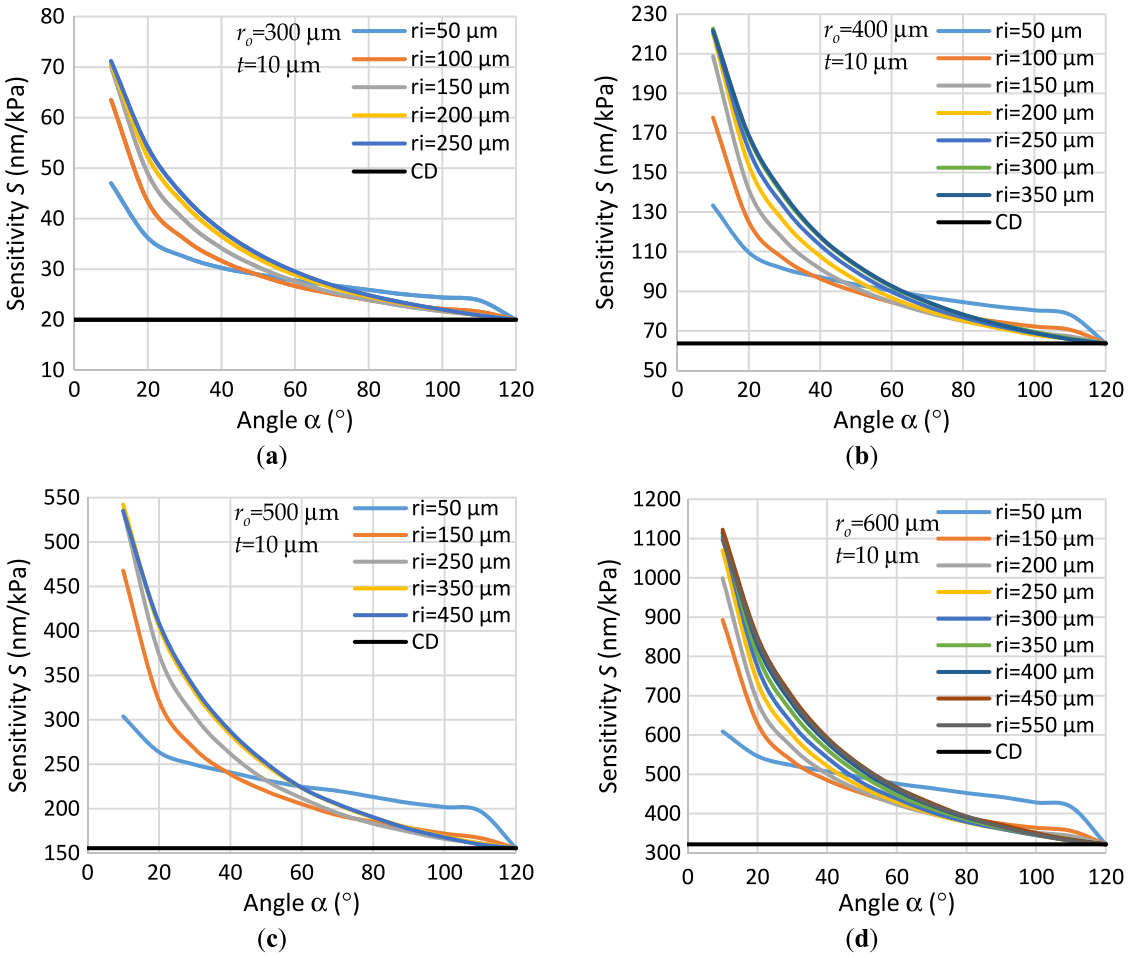

Fig. 3. The Change of the sensitivity ratings of the TLC and the conventional Circular Diaphragms (CD) according to the angle at t = 10 μm thickness for different geometric parameters: (a) r_o = 300 μm; (b) r_o = 400 μm; (c) r_o = 500 μm; (d) r_o = 600 μm.

Table 2
Fundamental resonance frequency f (kHz) of TLC for $r_i = r_o/2$ and Circular Diaphragms (CD).

r_o (μm)	Thickness t = 5 μm		Thickness t = 10 μm		Thickness t = 15 μm		Thickness t = 20 μm	
	CD	TLC α = 10° to 120°	CD	TLC α = 10° to 120°	CD	TLC α = 10° to 120°	CD	TLC α = 10° to 120°
300	152.53	68.633–152.53	304.84	135.84–304.84	456.45	201.85–456.45	606.14	266.78–606.14
400	85.78	38.613–85.78	171.58	76.698–171.58	257.21	114.30–257.21	342.41	151.47–342.41
500	54.90	24.752–54.90	109.81	49.187–109.81	164.81	73.451–164.81	219.45	97.420–219.45
600	38.12	17.235–38.12	76.26	34.225–76.26	114.57	51.103–114.57	152.39	67.939–152.39
700	28.02	12.656–28.02	56.02	25.190–56.02	84.04	37.610–84.04	112.12	50.003–112.12

frequency and the thickness. As the outer radius value increase, the frequency decreases and there is a proportion of $f \propto 1/r_o^2$ between the frequency and the outer radius. This is also compatible with Eq. (3), which is applied to conventional circular diaphragms. The effect of the thickness and radius on the natural frequency for the circular diaphragm is also valid for the TLC diaphragm. When the inner radius is chosen to be equal to half of the outer radius or greater than half of the outer radius, $r_i \geq r_o/2$, the results are come close to each other. From the numerical results obtained, it is determined that there is a proportion of $f \propto \alpha^{1/3}$ between the leaf angle and frequency. Also, when inner radius is equal to half of outer radius, i.e. $r_i = r_o/2$, the dynamic range gets the highest value. These interpretations are also valid for diaphragms with thickness of 5 μm and 20 μm. By changing these parameters, diaphragms with a wide range of frequency values have been created. This situation is shown in Table 2. For example, the first row of Table 2 points out that the frequency response for t = 5 μm and r_o = 300 μm can be tuned from 68.633 kHz to 152.53 kHz for TLC diaphragm while it remains constant at 152.53 kHz for CD diaphragm.

3.3. Effect of material properties on diaphragm performance

After the effects of the geometric dimensions on the sensitivity and the frequency response were determined, the analysis was performed by using the circular diaphragm equations to find out the effect of the material properties of the diaphragm. For this purpose, the results of the pre-made static structural analysis using SiO_2 and the contribution of the material properties in Eq. (1) were used as seen in Eq. (4):

$$S_{SiO_2} = \frac{d_{SiO_2}}{P} = \frac{3\left(1-\upsilon_{SiO_2}^2\right)r^4}{16E_{SiO_2}t^3} = \frac{3r^4}{16t^3} \times \frac{1-\upsilon_{SiO_2}^2}{E_{SiO_2}} = a \times \frac{1-\upsilon_{SiO_2}^2}{E_{SiO_2}} \quad (4)$$

where a, represents a constant which is only depending on the geometrical dimensions. The analysis results for SiO_2 were normalized by

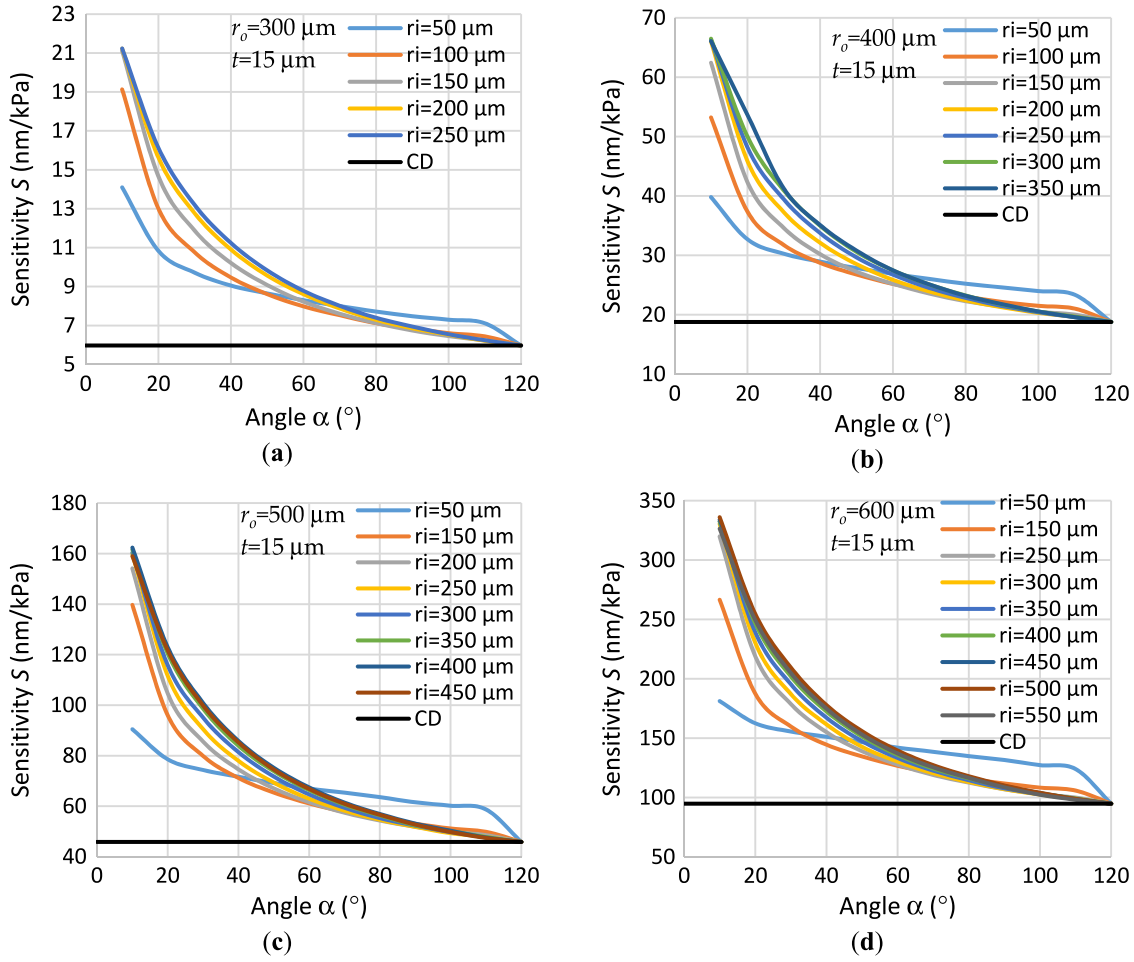

Fig. 4. The Change of the sensitivity ratings of the TLC and the conventional Circular Diaphragms (CD) according to the angle at t = 15 μm thickness for different geometric parameters: (a) r_o = 300 μm; (b) r_o = 400 μm; (c) r_o = 500 μm; (d) r_o = 600 μm.

dividing into SiO_2 material properties (E = 73 GPa, υ = 0.17, ρ = 2200 kg/m^3, [32]). Subsequently, when the value of SiO_2 sensitivity is divided by the values of SiO_2 and the result is multiplied by the values of silicon (Si) (E = 163 GPa, υ = 0.27, ρ = 2330 kg/m^3, [33]):, the sensitivity value of Si is obtained. This is given in Eq. (5).

$$S_{Si} = \frac{S_{SiO_2}}{\frac{1-\upsilon_{SiO_2}^2}{E_{SiO_2}}} \times \frac{1-\upsilon_{Si}^2}{E_{Si}} \tag{5}$$

The consistency of this approach according to the numerical results will give us an important way to understand the effects of material properties.

Eq. (5) was tested with FEM results by using different geometric dimensions for the TLC diaphragm and the errors for Eq. (5) are under 2%. These results were shown with error bars in Fig. 7. The average error was found to be 1.03%.

To understand the effects of material properties on sensitivity, we repeated the analyzes regarding the frequency response. For this, the results of the pre-made the modal analysis using SiO_2 and the contribution of the material properties in Eq. (3) were used:

$$f_{SiO_2} = \frac{10.21t}{2\pi r^2}\sqrt{\frac{E_{SiO_2}}{12\rho_{SiO_2}(1-\upsilon_{SiO_2}^2)}} = \frac{10.21t}{2\sqrt{12}\pi r^2}\sqrt{\frac{E_{SiO_2}}{\rho_{SiO_2}(1-\upsilon_{SiO_2}^2)}} = b \times \sqrt{\frac{E_{SiO_2}}{\rho_{SiO_2}(1-\upsilon_{SiO_2}^2)}} \tag{6}$$

where b represents a constant, which is only depending on the geometrical dimensions. The analysis results for SiO_2 were normalized by dividing into SiO_2 material properties. Then, we obtain the natural frequency value of Si when the result is multiplied by the values of silicon (Si):

$$f_{Si} = \frac{f_{SiO_2}}{\sqrt{\frac{E_{SiO_2}}{\rho_{SiO_2}(1-\upsilon_{SiO_2}^2)}}} \times \sqrt{\frac{E_{Si}}{\rho_{Si}(1-\upsilon_{Si}^2)}} \tag{7}$$

The Eq. (7) approach was tested with FEM results by using different geometric dimensions for the TLC diaphragm and the errors for Eq. (7) are under 1%. These results were shown with error bars in Fig. 8. The average error was found to be 0.22%.

Table 3
Effects of t, r_o, α and material properties on S and f.

	t	r_o	α	Material properties
Sensitivity (S)	$\propto 1/t^3$	$\propto {r_o}^4$	$\propto 1/\sqrt{\alpha}$	$\propto \frac{1-\upsilon^2}{E}$
Fundamental frequency (f)	$\propto t$	$\propto 1/{r_o}^2$	$\propto \alpha^{1/3}$	$\propto \sqrt{\frac{E}{\rho(1-\upsilon^2)}}$

3.4. An approach for TLC diaphragm

An approach that does not require multiple simulation processes for TLC diaphragms by combining all the analysis results from Sections 3.1–3.3 is developed in this section. Table 3 summarizes the effects of TLC diaphragm parameters on diaphragm sensitivity and fundamental frequency response.

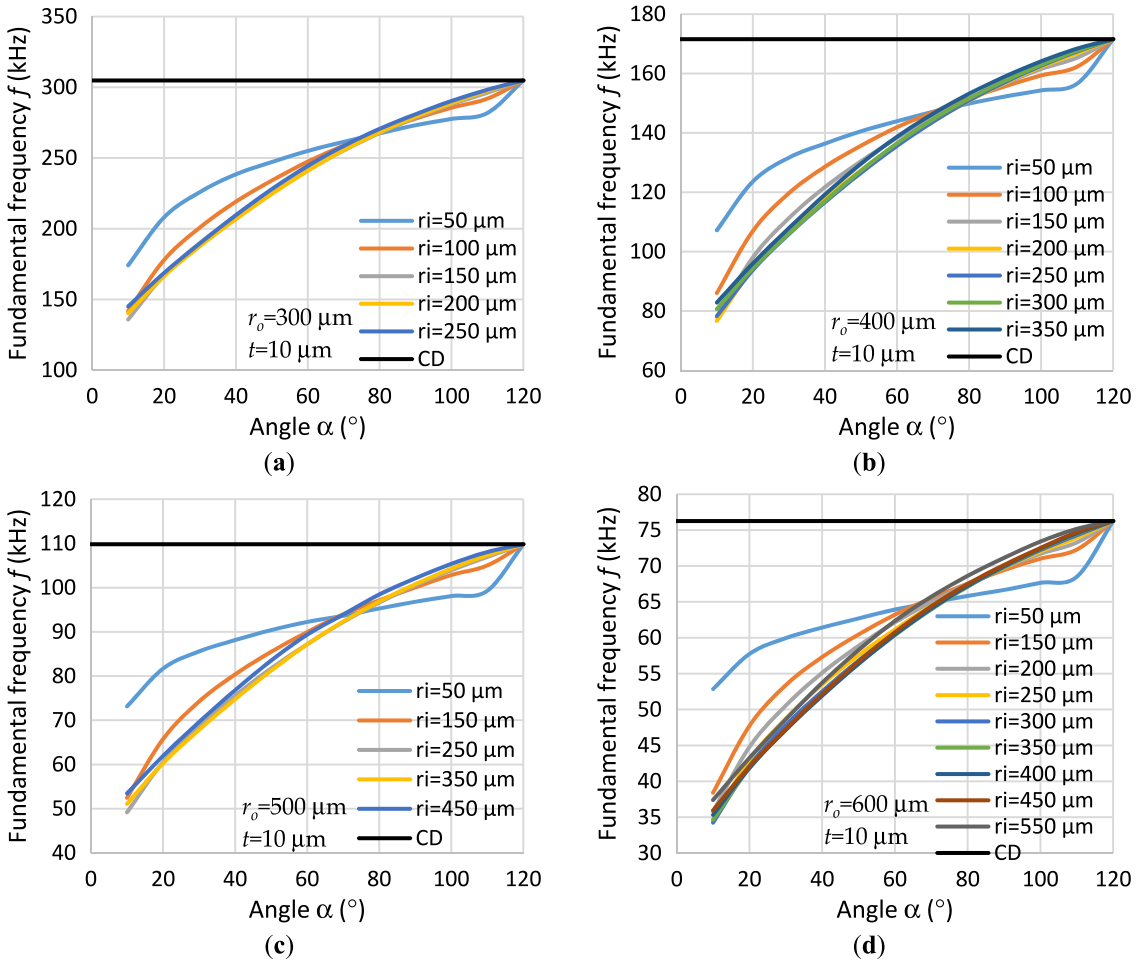

Fig. 5. The frequency response of the TLC and the conventional Circular Diaphragms (CD) according to the angle at t = 10 µm thickness for different geometric parameters: (a) r_o = 300 µm; (b) r_o = 400 µm; (c) r_o = 500 µm; (d) r_o = 600 µm.

When the condition of $r_i = r_o/2$ mentioned in Section 3.1 is met, the dynamic range is maximized, conditions of $S \propto 1/\sqrt{\alpha}$ and $f \propto \alpha^{1/3}$ are derived, and also, design simplicity is established. Eqs. (8) and (9) show the expressions for the sensitivity and fundamental frequency response of the regression analysis (R^2 = 0.9988 for sensitivity and R^2 = 0.9989 for fundamental frequency) on the static structural and modal analysis results with different t, r_o and α values from the TLC constructions satisfying the condition $r_i = r_o/2$.

$$S_{TLC} = \frac{d_{TLC}}{P} = \frac{3\left(1-\upsilon^2\right) r_o^4}{16Et^3\sqrt{\alpha/120°}}; r_i = r_o/2 \tag{8}$$

$$f_{TLC} = \frac{10.21t(\alpha/120°)^{1/3}}{2\pi r_o^2}\sqrt{\frac{E}{12\rho(1-\upsilon^2)}}; r_i = r_o/2 \tag{9}$$

Eqs. (8) and (9) are the most important contributions of our work because they can represent the sensitivity and fundamental frequency of a tunable diaphragm with a simple but effective way. In order to see the utility ranges of Eqs. (8) and (9), we generated S and f values for different parameters selected over a wide range. FEM analyzes of TLC structures with the same geometry were also performed and the results were compared in Figs. 9 and 10 with error bars. The average error was found to be 2.38% and 0.22% for the sensitivity and the fundamental frequency response, respectively. Note that, our main goal in this work was to present a simple way for design purposes. Eqs. (8) and (9) have been obtained after 1488 3d drawings and 2976 total computations belonging to the drawings. We hope these computations will help to an easy MEMS fabrication.

Eqs. (10) and (11) represent the upper boundary conditions of Eqs. (8) and (9) for values of the leaf angle.

$$\lim_{\alpha\to 120°} S_{TLC} = S_{circular} \tag{10}$$

$$\lim_{\alpha\to 120°} f_{TLC} = f_{circular} \tag{11}$$

When the boundary condition of $\alpha = 120°$ is satisfied, TLC approximates to the conventional circular structure. As can be shown in Figs. 9 and 10, S and f values are overlapped when α goes to 120° . On the other hand, when the leaf angle, α, goes to the lower limit of 5° , the following relationships exist:

$$\lim_{\alpha\to 5°} S_{TLC} = 5 \times S_{circular} \tag{12}$$

$$\lim_{\alpha\to 5°} f_{TLC} = \frac{f_{circular}}{3} \tag{13}$$

In this case, when the FEM results were compared with the results of the approach proposed in this work, the average errors were less than 2.5% for the sensitivity and less than 0.5% for the fundamental frequency response, respectively.

Our calculations show that sensitivity and the frequency response the measurement range can be tuned between 2.53–15913 nm/kPa, 12.656–606.14 kHz, respectively. Also, the measurement range can be adjusted from 0.1 Pa for FP cavity length change of 1.59 nm to 2.37 MPa for the diaphragm's mechanical strength limit of 6 µm. Generally, in order to ensure the linearity of the deflection at the center point, the deflection amount should be less than 30% of the diaphragm thickness [34].

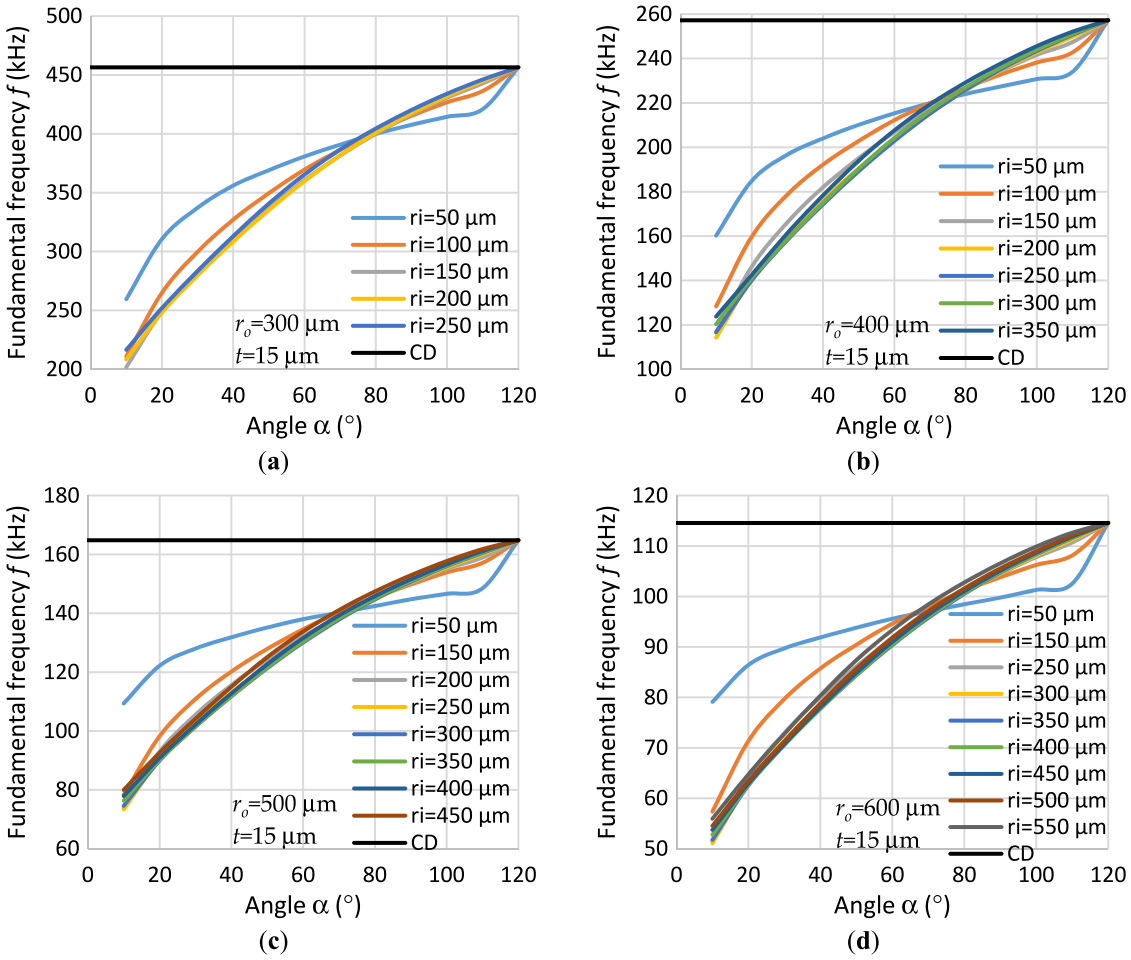

Fig. 6. The frequency response of the TLC and the conventional Circular Diaphragms (CD) according to the angle at t = 15 μm thickness for different geometric parameters: (a) r_o = 300 μm; (b) r_o = 400 μm; (c) r_o = 500 μm; (d) r_o = 600 μm.

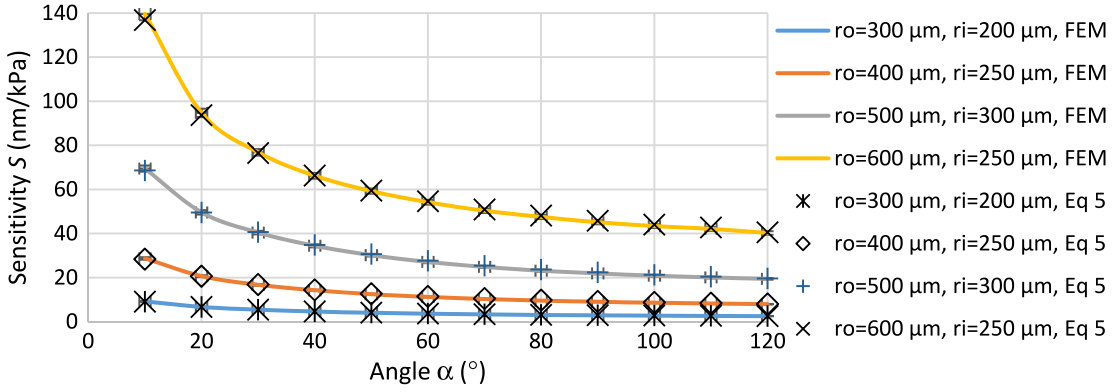

Fig. 7. Sensitivity values obtained for Si using Silica's results and comparison of FEM results (error bars represent less than 2% error).

4. Conclusions

For the first time in the literature, we proposed that a TLC-shaped diaphragm geometry would provide significant advantages to be able to design simplicity for the diaphragm-based EFPI fiber acoustic pressure sensors. For this purpose, we have achieved a wider operating range by increasing the number of parameters used in tuning, so that the sensor can precisely respond to the physical parameter being measured. We have analyzed both the sensitivity and the frequency response of this new structure using finite element method and numerical analysis techniques. As a result of the analyzes, it has been shown that we can increase the sensitivity of the acoustic sensor by about 5 times without changing the diameter and thickness when we converted a circular diaphragm to TLC diaphragm. In addition, the sensor can be capable of taking a value up to 1/3 of its original fundamental resonance frequency value and narrow band sensors can be acquired which can operate at values close to the desired frequency value. Many researchers who design diaphragm-based sensor for acoustic

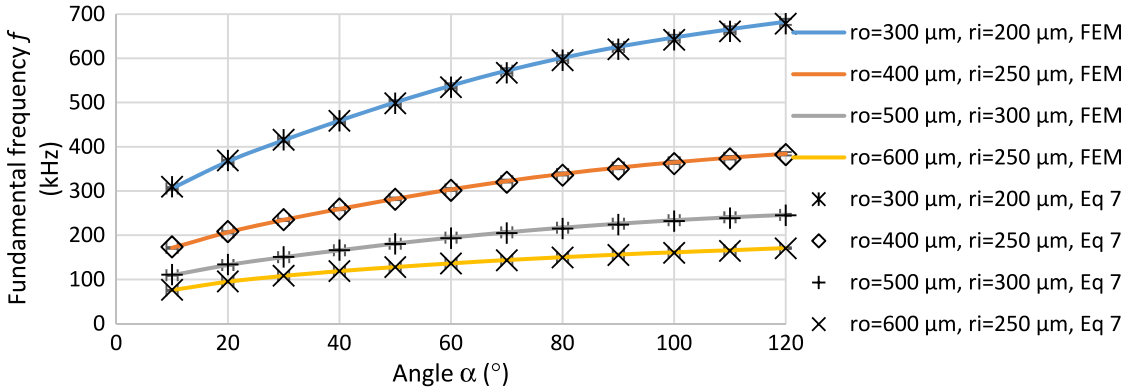

Fig. 8. The frequency response obtained for Si using Silica's results and comparison of FEM results (error bars represent less than 1% error).

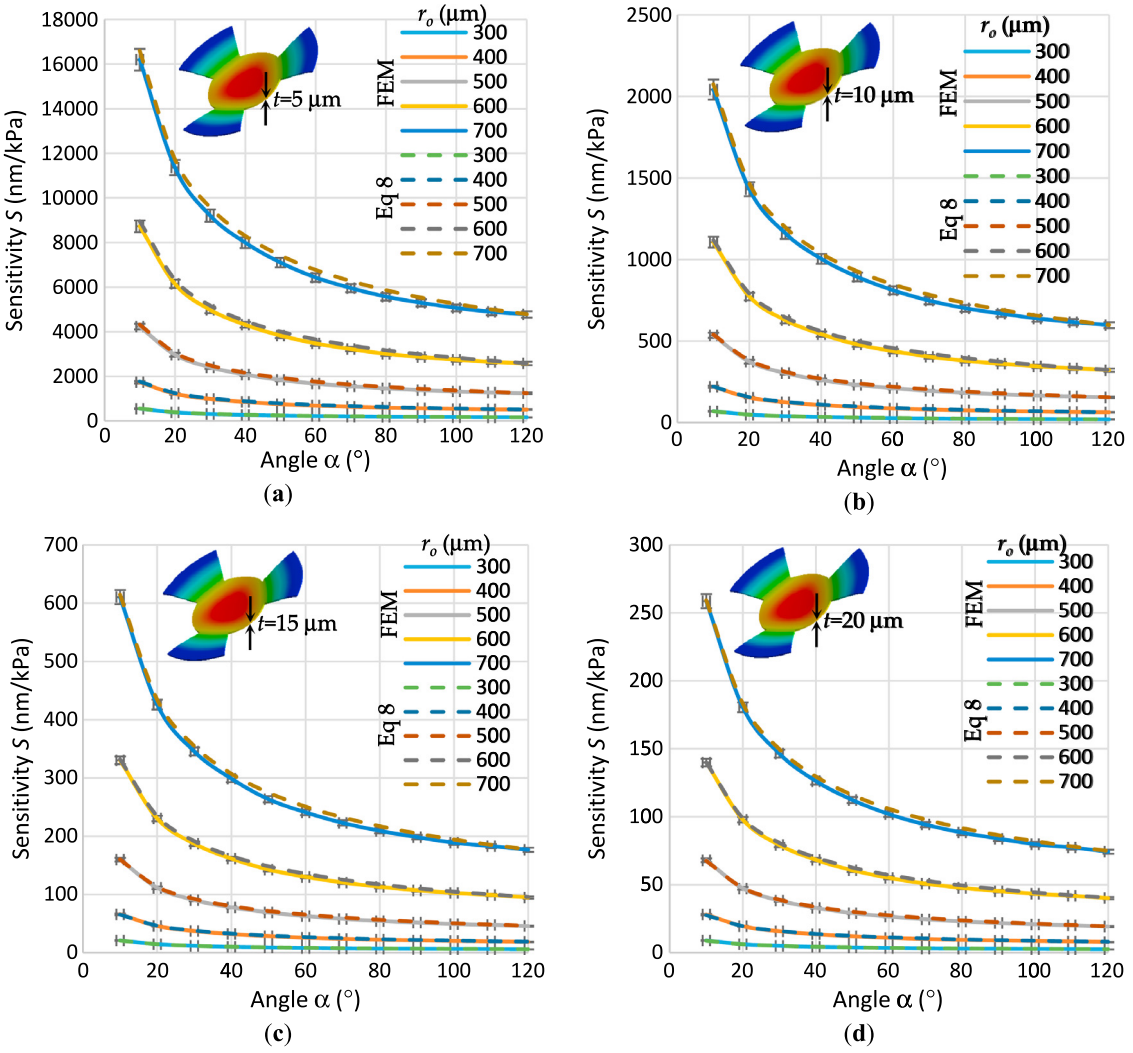

Fig. 9. Comparisons of sensitivity values of TLC diaphragm in different r_o values with FEM and Eq. (8). (a) t = 5 μm with 3% error bars; (b) t = 10 μm with 3% error bars; (c) t = 15 μm with 2% error bars; (d) t = 20 μm with 2% error bars.

pressure benefit from the analytical models of circular diaphragms in the literature. For this reason, we have obtained sensitivity and natural frequency approaches for TLC-like structures. We compared the obtained approaches with the FEM-based simulation results. In addition, since TLC will provide pressure balance of the sensor tip because of its geometrical structure, it does not be required to drill holes on the sensor tips.

Acknowledgments

This work was supported by the Research Fund of the Erciyes University, Turkey. Project numbers FDK-2016-6811 and FDK-2016-6815. The authors would like to thank Erciyes University Clinical Engineering Research and Application Center for their supports in the research activities among the staffs.

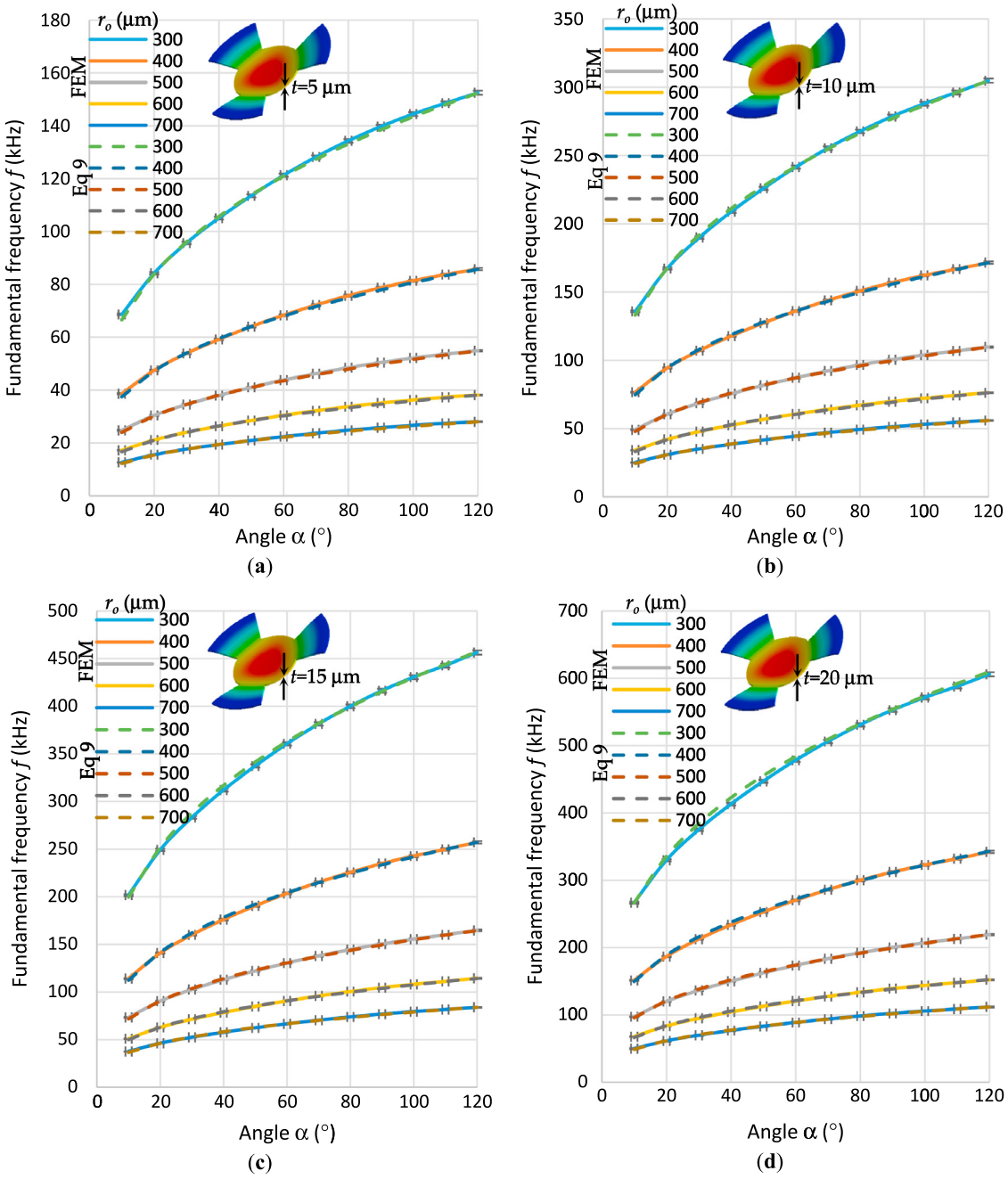

Fig. 10. Comparisons of fundamental resonance frequency response of TLC diaphragm in different r_o values with FEM and Eq. (9) (error bars represent less than 0.5% error). (a) t = 5 μm; (b) t = 10 μm; (c) t = 15 μm; (d) t = 20 μm.

Author Contributions

O.G.S. gave the main idea; S.E.H. and T.E.T. performed the analyzes and wrote the paper.

Conflict of interest

The authors declare no conflict of interest.

References

[1] S. Poeggel, D. Tosi, D. Duraibabu, G. Leen, D. McGrath, E. Lewis, Optical fibre pressure sensors in medical applications, Sensors 15 (7) (2015) 17115–17148. http://dx.doi.org/10.3390/s150717115.

[2] Y. Li, W. Zhang, Z. Wang, H. Xu, F. Li, A Low-Cost All-Silica Fabry–Perot Pressure Sensor for Biomedical Applications. International Photoacoustic and OptoElectronics Meetings, Wuhan, China, 18-21 June 2014. FF4B-7, 10.1364/FBTA.2014.FF4B.7.

[3] Z. Gong, K. Chen, Y. Yang, X. Zhou, Q. Yu, Photoacoustic spectroscopy based multi-gas detection using high-sensitivity fiber-optic low-frequency acoustic sensor, Sensors Actuators B 260 (2018) 357–363. http://dx.doi.org/10.1016/j.snb.2018.01.005.

[4] Z. Gong, K. Chen, Y. Yang, X. Zhou, W. Peng, Q. Yu, High-sensitivity fiber-optic acoustic sensor for photoacoustic spectroscopy based traces gas detection, Sensors Actuators B 247 (2017) 290–295. http://dx.doi.org/10.1016/j.snb.2017.03.009.

[5] Q. Wang, J. Wang, L. Li, Q. Yu, An all-optical photoacoustic spectrometer for trace gas detection, Sensors Actuators B 153 (1) (2011) 214–218. http://dx.doi.org/10.1016/j.snb.2010.10.035.

[6] D.B. Duraibabu, S. Poeggel, E. Omerdic, R. Capocci, E. Lewis, T. Newe, G. Dooly, An Optical Fibre Depth (Pressure) Sensor for Remote Operated Vehicles in Underwater Applications, Sensors 17 (2) (2017) 406. http://dx.doi.org/10.3390/s17020406.

[7] F. Wang, Z. Shao, J. Xie, Z. Hu, H. Luo, Y. Hu, Extrinsic Fabry–Pérot underwater acoustic sensor based on micromachined center-embossed diaphragm, J. Lightwave Technol. 32 (23) (2014) 4026–4034. http://dx.doi.org/10.1109/JLT.2014.2362494.

[8] W. Wang, Q. Yu, X. Jiang, High sensitivity diaphragm-based extrinsic Fabry–Perot interferometric optical fiber underwater ultrasonic sensor, Adv. Mater. Rapid Commun. 6 (2012) 697–702. http://dx.doi.org/10.1007/s12647-013-0054-0.

[9] H. Liao, P. Lu, L. Liu, S. Wang, W. Ni, X. Fu, J. Zhang, Phase Demodulation of Short-Cavity Fabry–Perot Interferometric Acoustic Sensors With Two Wavelengths, IEEE Photonics J. 9 (2) (2017) 1–9. http://dx.doi.org/10.1109/JPHOT.2017.2689771.

[10] S. Wang, P. Lu, L. Liu, H. Liao, Y. Sun, W. Ni, H. Xu, An infrasound sensor based on extrinsic fiber-optic Fabry–Perot interferometer structure, IEEE Photonics Technol. Lett. 28 (11) (2016) 1264–1267. http://dx.doi.org/10.1109/LPT.2016.2538318.

[11] Q. Rong, Y. Hao, R. Zhou, X. Yin, Z. Shao, L. Liang, X. Qiao, UW Imaging of seismic-physical-models in air using fiber-optic Fabry–Perot Interferometer, Sensors 17 (2) (2017) 397. http://dx.doi.org/10.3390/s17020397.

[12] Y. Sun, G. Feng, G. Georgiou, E. Niver, K. Noe, K. Chin, Center embossed diaphragm design guidelines and Fabry–Perot diaphragm fiber optic sensor, Microelectron. J. 39 (5) (2008) 711–716. http://dx.doi.org/10.1016/j.mejo.2007.12.020.

[13] X. Mao, S. Yuan, P. Zheng, X. Wang, Stabilized Fiber-Optic Fabry–Perot Acoustic Sensor Based on Improved Wavelength Tuning Technique, J. Lightwave Technol. 35 (11) (2017) 2311–2314. http://dx.doi.org/10.1109/JLT.2017.2651151.

[14] J. Ma, H. Xuan, H.L. Ho, W. Jin, Y. Yang, S. Fan, Fiber-optic Fabry–Perot acoustic sensor with multilayer graphene diaphragm, IEEE Photonics Technol. Lett. 25 (10) (2013) 932–935. http://dx.doi.org/10.1109/LPT.2013.2256343.

[15] Q. Wang, Z. Ma, Feedback-stabilized interrogation technique for optical Fabry–Perot acoustic sensor using a tunable fiber laser, Opt. Laser Technol. 51 (2013) 43–46. http://dx.doi.org/10.1016/j.optlastec.2013.03.019.

[16] B. Liu, J. Lin, H. Liu, Y. Ma, L. Yan, P. Jin, Diaphragm based long cavity Fabry–Perot fiber acoustic sensor using phase generated carrier, Opt. Commun. 382 (2017) 514–518. http://dx.doi.org/10.1016/j.optcom.2016.08.013.

[17] W. Wang, S. Li, L. Wen, Ultra-low sensitivity to temperature low-cost optical fiber Fabry–Perot micro pressure sensor with a chitosan diaphragm, Opt. Commun. 309 (2013) 302–306. http://dx.doi.org/10.1016/j.optcom.2013.07.076.

[18] F. Xu, D. Ren, X. Shi, C. Li, W. Lu, L. Lu, B. Yu, High-sensitivity Fabry–Perot interferometric pressure sensor based on a nanothick silver diaphragm, Opt. Lett. 37 (2) (2012) 133–135. http://dx.doi.org/10.1364/OL.37.000133.

[19] J. Eom, C.J. Park, B.H. Lee, J.H. Lee, I.B. Kwon, E. Chung, Fiber optic Fabry–Perot pressure sensor based on lensed fiber and polymeric diaphragm, Sensors Actuators A 225 (2015) 25–32. http://dx.doi.org/10.1016/j.sna.2015.01.023.

[20] B. Liu, J. Lin, H. Liu, A. Jin, P. Jin, Extrinsic Fabry–Perot fiber acoustic pressure sensor based on large-area silver diaphragm, Microelectron. Eng. 166 (2016) 50–54. http://dx.doi.org/10.1016/j.mee.2016.09.005.

[21] L. Cheng, L. Qianwen, G. Tingting, X. Jun, F. Shangchun, J. Wei, An ultra-high sensitivity Fabry–Perot acoustic pressure sensor using a multilayer suspended graphene diaphragm. Sensors, 2015 IEEE, Busan, South Korea, 1-4 Nov. 2015, 15717290, pp. 1-4, 10.1109/ICSENS.2015.7370318.

[22] Z. Gong, K. Chen, X. Zhou, Y. Yang, Z. Zhao, H. Zou, Q.X. Yu, High-sensitivity fabry–perot interferometric acoustic sensor for low-frequency acoustic pressure detections, J. Lightwave Technol. 35 (24) (2017) 5276–5279. http://dx.doi.org/10.1109/JLT.2017.2761778.

[23] X. Wang, B. Li, Z. Xiao, S.H. Lee, H. Roman, O.L. Russo, K.R. Farmer, An ultra-sensitive optical MEMS sensor for partial discharge detection, J. Micromech. Microeng. 15 (3) (2004) 521. http://dx.doi.org/10.1088/0960-1317/15/3/012.

[24] X. Wang, B. Li, O.L. Russo, H.T. Roman, K.K. Chin, K.R. Farmer, Diaphragm design guidelines and an optical pressure sensor based on MEMS technique, Microelectron. J. 37 (1) (2006) 50–56. http://dx.doi.org/10.1016/j.mejo.2005.06.015.

[25] J. Deng, H. Xiao, W. Huo, M. Luo, R. May, A. Wang, Y. Liu, Optical fiber sensor-based detection of partial discharges in power transformers, Opt. Laser Technol. 33 (5) (2001) 305–311. http://dx.doi.org/10.1016/S0030-3992(01)00022-6.

[26] M.S. Ferreira, P. Roriz, S.O. Silva, J.L. Santos, O. Frazão, Next generation of Fabry–Perot sensors for high-temperature, Opt. Fiber Technol., Mater. Devices Syst. 19 (6) (2013) 833–837. http://dx.doi.org/10.1016/j.yofte.2013.07.006.

[27] L. Liu, P. Lu, S. Wang, X. Fu, Y. Sun, D. Liu, Q. Yao, UV adhesive diaphragm-based FPI sensor for very-low-frequency acoustic sensing, IEEE Photonics J. 8 (1) (2016) 1–9. http://dx.doi.org/10.1109/JPHOT.2015.2509866.

[28] V.R. Singh, J. Miao, Z. Wang, G. Hegde, A. Asundi, Dynamic characterization of MEMS diaphragm using time averaged in-line digital holography, Opt. Commun. 280 (2) (2007) 285–290. http://dx.doi.org/10.1016/j.optcom.2007.08.030.

[29] J. Xu, X. Wang, K.L. Cooper, A. Wang, Miniature all-silica fiber optic pressure and acoustic sensors, Opt. Lett. 30 (24) (2005) 3269–3271. http://dx.doi.org/10.1364/OL.30.003269.

[30] S.E. Lima, O. Frazão, F.M. Araújo, L.A. Ferreira, V. Miranda, J.L. Santos, Extrinsic and intrinsic fiber optic interferometric sensors for acoustic detection in high-voltage environments, Opt. Eng. 48 (2) (2009) 024401. http://dx.doi.org/10.1117/1.3080752.

[31] C. Fu, W. Si, H. Li, D. Li, P. Yuan, Y. Yu, A Novel High-Performance Beam-Supported Membrane Structure with Enhanced Design Flexibility for Partial Discharge Detection, Sensors 17 (3) (2017) 593. http://dx.doi.org/10.3390/s17030593.

[32] J. Ma, Miniature Fiber-Tip Fabry–Perot Interferometric Sensors for Pressure and Acoustic Detection (Doctoral dissertation), The Hong Kong Polytechnic University, 2014. http://hdl.handle.net/10397/7136.

[33] A MEMS Clearinghouse® and information portal for the MEMS and Nanotechnology community. Available online: https://www.memsnet.org/material/siliconsibulk/ (20.04.2018).

[34] D. Giovanni, Flat and Corrugated Diaphragm Design Handbook, vol. 11, first ed., CRC Press, 1982.